ORIGINAL PAPER

Experimental study on the influence of tangential stress gradient on the energy evolution of strainburst

Xiqi Liu[1] · Yuanyou Xia[1] · Manqing Lin[2] · Gang Wang[1] · Dongxing Wang[3]

Abstract
Strainburst is a kind of safety concern caused by the release of elastic strain energy from surrounding rocks under a tangential stress gradient. In this paper, laboratory rockburst model tests under four different stress gradients were conducted. Based on the acoustic emission (AE) data, the influence of tangential stress gradient on the energy evolution of strainburst was studied. The results indicate that (1) by controlling the tangential stress gradient loading at the top of the specimen, the change process of tangential and radial stress gradient from surrounding rocks caused by excavation disturbance, to a large extent, can be simulated. (2) The failure phenomena and failure stress of the specimen are both related to its tangential stress gradient distribution. As the tangential stress gradient increases, the failure stress is reduced, but dynamic failure phenomena become more evident. (3) With the increase of tangential stress gradient, the accumulation period of elastic strain energy lengthens, whereas the dissipation and release periods shorten during the loading process. As the tangential stress gradient rises, when the specimen rockburst occurs, the more dramatic decrease and faster decreasing rate of AE b-value reveal the increase in the specimen's proportion of shear failure. Also, the critical index (r) of probability density distribution shows a downward trend, which indicates that the AE energy in the low disturbance area decreases. In contrast, the AE energy span in the high disturbance area widens and the energy level becomes higher.

Keywords Strainburst · Tangential stress gradient · Model test · Acoustic emission · Energy

Introduction

The exploitation of resources and the expansion of large-scale water conservancy and hydropower projects in the deep underground have resulted in the increasingly prominent geological disasters caused by high geo-stress, which bring severe challenges to the safe construction of deep underground space (Feng et al. 2017; Kaiser et al. 2001, 2015; Simser 2019; Zhou

✉ Yuanyou Xia
   xiayy1965@whut.edu.cn

✉ Manqing Lin
   manqing_lin@foxmail.com

1   School of Civil Engineering and Architecture, Wuhan University of Technology, Wuhan 430070, Hubei, China

2   School of Resources and Safety Engineering, Wuhan Institute of Technology, Wuhan 430070, Hubei, China

3   Key Laboratory of Geotechnical and Structural Engineering Safety of Hubei Province, School of Civil Engineering, Wuhan University, Wuhan 430070, Hubei, China

et al. 2020). During the construction of underground engineering, the rock mass stress in the three-dimensional compression state redistributes due to excavation. During this process, the energy inside the rock also accumulates, dissipates, and transmits. Some of the energy dissipates in the development and propagation of cracks in surrounding rock, and some is stored as strain energy or potential energy. As the elastic strain energy accumulated in the surrounding rock increases to a certain extent, it would be converted into the kinetic energy of the spalling rock block, resulting in rockburst (Li et al. 2019). Therefore, the rockburst mechanism can be fundamentally studied by analyzing the influence of rock stress on its internal energy storage, dissipation, and transmission during underground engineering excavation.

The failure of an underground rock structure is a synthetic process of energy dissipation and energy release (Zhang et al. 2018). In its early stage of deformation, the rock mass stores the energy provided by the outside in the form of elastic strain energy and dissipates it to the outside through damage evolution, etc. In contrast, in the later stage of deformation, it is mainly released dramatically. Mansurov (2001) defined

🖄 Springer

the evolution law of the rockburst fracture process and the relationship between energy and fracture. G. Brauner (Peng et al. 2014) proposed the theory of energy rate, which took into account the conditions that each part of the energy needed to be satisfied when rockburst occurred, reflected the time effect of rockburst through the rate of the time change, and explained the power source. However, it is still challenging to explain the mechanisms of rockburst due to the limitation of nonlinear problems in theory. Therefore, many scholars have endeavored to reproduce the phenomena of rockburst by simulating the stress characteristics of surrounding rocks under laboratory conditions, so as to study rockburst mechanism. Based on the stress state change of surrounding rocks before and after excavation, loading tests with one free face under the true-triaxial condition were performed to simulate the rockburst (He et al. 2012, 2015a; Si and Gong 2020). Feng et al. (2016) and He et al. (2015b) simulated the process of excavation unloading and stress concentration of surrounding rock mass through three principal stress directions loading, one side rapid unloading, and top uniform loading and analyzed the failure and energy characteristics of specimen rockburst at each phase. Chen et al. (2019) studied the energy dissipation process of debris under different loading rates through the true-triaxial test. Zhai et al. (2020) investigated the fracture evolution during rockbursts of granodiorite and basalt that appeared to be representatives of two different rockburst modes under true-triaxial loading using AE analysis. Su et al. (2017a, 2017b) studied the influence of different disturbance loads and loading rates on rockburst through the true-triaxial test and revealed rockburst's energy evolution process through multiple approaches such as energy transformation analysis and energy consumption analysis of rockburst debris.

Nevertheless, in practical engineering, rockburst is a kind of disaster caused by tangential stress gradient from surrounding rocks (Qian 2014). The in-excavated underground rock mass is in the state of three principal stresses, and the excavation unloading provides a free surface for the rock damage. The tangential stress (σ_1) on the cavern walls is more considerable, which decreases gradually towards the inside of surrounding rocks with a specific gradient. In contrast, the radial stress (σ_3) equals 0 on the walls, which yet increases towards the inside of surrounding rocks. Therefore, Huo et al. (2020) and Liu et al. (2019) preliminarily explored the rockburst characteristics of the specimen under true-triaxial tangential gradient stress and found that with the increase of the tangential stress gradient, the rockburst intensity shows an increasing trend. However, the influence of tangential stress gradient on rockburst energy evolution has not been reported ever. Therefore, to further analyze the influence mechanisms and rules from the perspective of energy, a true-triaxial gradient and hydraulic-pneumatic composite loading apparatus was adopted in this paper to conduct the rockburst test under 4

different tangential stress gradients. Combined with the failure phenomenon and AE signals monitored during specimen rockburst, the influence of tangential stress gradient on the energy evolution of the specimen during rockburst was studied, which is of significance to understand the rockburst failure mechanisms and improve the accuracy of its prediction.

Experimental procedures

Rockburst test system

In the rockburst model test, a true-triaxial gradient and hydraulic-pneumatic composite loading apparatus was adopted (specimen size: 400mm×600mm×1000mm), which is mainly composed of 4 parts: the main engine, the pneumatic control system, the hydraulic control system, and the monitoring system, as shown in Fig. 1. Its maximum loading capacity is 20MPa, which could realize the special function of three principal stress directions loading (simulating the in situ stress state), one side rapid unloading (simulating excavation behavior), and top gradient loading (simulating tangential stress concentration). The monitoring system consists of the AE test instrument, the stress monitoring instrument, and the camera. AE signal acquisition threshold is set as 40dB, and the sampling frequency is 1MHz. The monitoring range of the strain brick is 0~60MPa, and it is buried in the center of 4 equal areas at the top of the specimen, which could monitor the change process of three principal stress at four tangential gradient stress loading positions. The stress data were obtained by the static strain acquisition instrument. The spatial arrangement of AE probe and strain brick is shown in Fig. 2.

Specimen materials and preparation

The physical and mechanical properties of the selected specimen materials should meet the brittleness and rockburst tendency indicators, but other physical and mechanical parameters of the materials are not required to meet the strict similarity ratio (Zhou et al. 2015). In the experiment, α-hemihydrate gypsum was selected as a similar material to simulate deep rock mass (Hou et al. 2018). As shown in Fig. 3 and Fig. 4, mechanical parameters of the material were determined through the uniaxial and three-point bending tests of samples with different water-gypsum ratios, and the ratio that meets the conditions of rockburst test was selected. The impact energy index W_{cf} (Wang et al. 2015), elastic modulus, and other relevant parameters are shown in Table 1.

Based on the ratio shown in Table 1, rectangular specimens with the size of 400mm×600mm×1000mm were made according to the requirements of the rockburst apparatus. After dried at room temperature, the specimens were fed into the loading chamber of the instrument. Furthermore, to minimize

Fig. 1 Rockburst test equipment
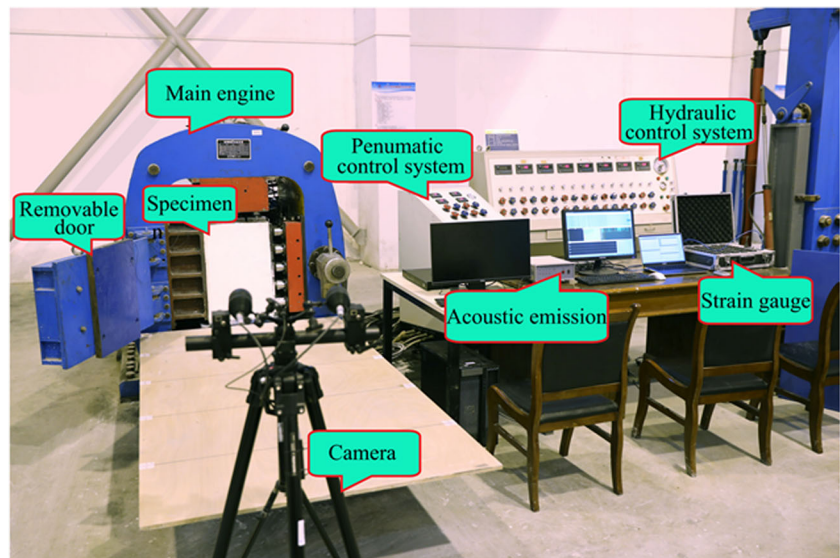
the influence of lateral friction on boundary conditions during loading processes, 2 layers of polymer with graphite powder were placed between each loading surface and the stress transferring platens.

Loading path

To figure out the influence of tangential stress gradients on rockburst energy evolution characteristics, the simplified Eq. (1) can be used to simulate the tangential stress of surrounding rock based on the distribution law of tangential stress of surrounding rock after excavation (Singh et al. 2011):

$$y = nae^{-mx} + c \tag{1}$$

where y is the tangential stress of a certain point in the surrounding rock, x is the distance from a certain point in the surrounding rock (inside the specimen) to the excavation
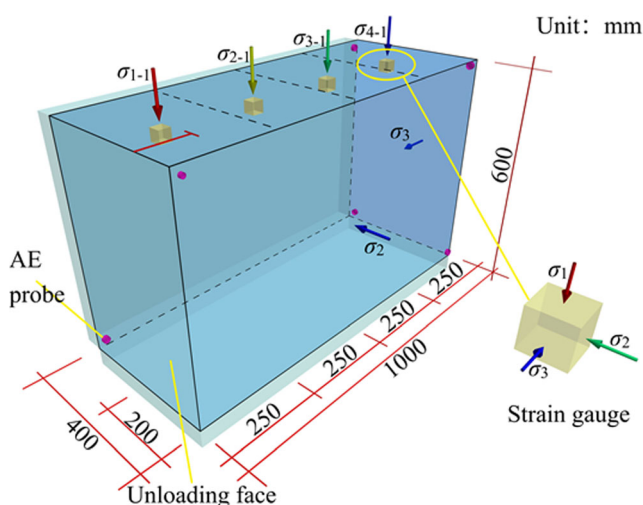

Fig. 2 AE probe and strain brick layout

boundary (unloading surface), n is the number of loading steps of tangential gradient stress, a is the stress loading stride of σ_{1-1}, c is the vertical stress of initial rock, and m is the tangential stress gradient coefficient.

According to the ground stress distribution in different countries (Brown and Hoek 1978; Liu et al. 2016), the ratio of vertical ground stress σ_V to horizontal ground stress σ_H is set as follows: $\sigma_V/\sigma_H=2$ ($\sigma_1=\sigma_V=c>\sigma_2=\sigma_3=\sigma_H$). First, each specimen was loaded with in situ stress in three principal directions ($\sigma_1=c=2$MPa, $\sigma_2=\sigma_3=1$MPa), as shown in Fig. 5a. Afterwards, the movable door plate in front of the equipment was quickly removed, leading to an abrupt release of stress from this plate and keeping constant the horizontal confining stress in other sides of the specimen to simulate the tunnel excavation. Simultaneously, the vertical load was applied step by step, as shown in Fig. 5b. Gradient 1 (σ_{1-1}, $x=0.0$m) increased in n steps with the stride of $a=0.5$MPa, and other tangential gradient stress were applied synchronously through $y=nae^{-mx}+c$ calculation (the stress of gradient 2/3/4 is signed as $\sigma_{1-2}/\sigma_{1-3}/\sigma_{1-4}$, corresponding to $x=0.25$m/0.5m/0.75m, respectively). The test used quasi-static compression loading, and the loading and pressure stabilization time of each step was 30min. In this paper, four different top gradient loading paths ($m=0, 2, 4, 6$) were used in the rockburst test. The time-history curves of loading paths are shown in Fig. 6.

Results analysis

Stress analysis in rockburst process

Figure 7 shows the time-history curve of the change of the three principal stress in different tangential gradient stress loading processes measured by the strain brick. In the moment
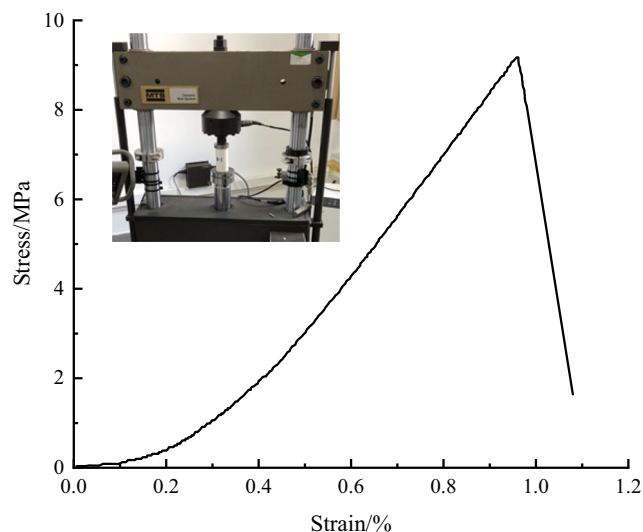
Table 1 Parameters of the specimen and the index of rockburst trend

Material	Water/gypsum ratio	Citric acid (g)/water (g)	Poisson's ratio	Elastic modulus/GPa	σ_c/ MPa	σ_t/ MPa	W_{cf}
Gypsum	0.7	0.12%	0.25	1.268	9.2	0.54	5.63

σ_c is uniaxial compressive strength; σ_t is uniaxial tensile strength; W_{cf} is the ratio of pre-peak area and post-peak area of the stress-strain curve of specimen material in a uniaxial compression test. $W_{cf} > 3$, strong rockburst; $3 \geq W_{cf} \geq 2$, weak rockburst; $W_{cf} < 2$, no rockburst

of specimen rockburst, the curve of the measured three principal stress (σ_1, σ_2, σ_3) changing with the distance of unloading surface is illustrated in Fig. 8. As shown in Fig. 7 and Fig. 8, $\sigma_{1\text{-}1}/\sigma_{1\text{-}2}/\sigma_{1\text{-}3}/\sigma_{1\text{-}4}$ are the measured stress values at the top σ_1 direction, $\sigma_{2\text{-}1}/\sigma_{2\text{-}2}/\sigma_{2\text{-}3}/\sigma_{2\text{-}4}$ are the measured stress values at the side σ_2 direction, and $\sigma_{3\text{-}1}/\sigma_{3\text{-}2}/\sigma_{3\text{-}3}/\sigma_{3\text{-}4}$ are the measured stress values at the σ_3 direction.

Compared with Fig. 6 and Fig. 7, it can be seen that the stress path measured by the model rockburst test is basically consistent with the test loading paths. As shown in Fig. 8, after simulating the excavation of surrounding rock, the tangential stress $\sigma_1 (\sigma_{1\text{-}1} \sim \sigma_{1\text{-}4})$ and the radial stress $\sigma_3 (\sigma_{3\text{-}1} \sim \sigma_{3\text{-}4})$ of the surrounding rocks are distributed in gradients. σ_3 is close to 0 at the unloading surface, while the axial stress $\sigma_2 (\sigma_{2\text{-}1} \sim \sigma_{2\text{-}4})$ remains essentially constant, which is consistent with the stress change law of surrounding rock after excavation, characterized by unloading of radial stress (σ_3) and an increase of tangential stress (σ_1) as well as the approximately unchanged intermediate stress (σ_2). Furthermore, it can be seen from the stress results of the test that when the 4 specimens fail, the maximum vertical loading stress $\sigma_{1\text{-}1}$ is lower than the σ_c of uniaxial compressive strength. This is consistent with the failure stress of most engineering rockburst when the maximum tangential stress $\sigma_{\theta max}$ is below or far below σ_c (Zhang et al. 2020).

The stress characteristics of the specimen indicate that the rockburst test method of three principal stress directions loading, one side rapid unloading, and top gradient loading can more truly simulate the stress evolutionary process of surrounding rock in high geo-stress area under the secondary stress field, which is reflected by the reduction of radial stress and the concentration of tangential stress after rock excavation.

Failure analysis of specimen

Although rockburst failure occurred in all the 4 specimens under different tangential gradient stress loading conditions, the failure phenomena were quite different. Figures 9, 10, 11, and 12 list the corresponding failure phenomena, and lateral crack propagation photos of specimens after rockburst are shown in Fig. 13.

Figure 9 and Fig. 10 show that when the tangential stress gradient of the specimen was small ($m=0$, $m=2$), the characteristics of the dynamic rockburst failure of the specimen are not noticeable, presented as flake debris spalling or breaking, and the debris was mainly distributed in the range of 0.5m near the free face of the specimen. As the tangential stress gradient increased ($m=4$), the debris were mainly angular and blocky, and the throwing distance was up to 0.9m, as shown in Fig. 11. With the tangential stress gradient coefficient m reaching 6, the debris were mostly wedge-shaped or block-shaped, and the maximum throwing distance was 1.7m, as shown in Fig. 12. It can be seen that with the increase of

Fig. 3 Uniaxial test results of specimen materials

Fig. 4 Three-point bending tests

Fig. 5 The stress state transformation of the surrounding rock masses before and after excavation. (**a**) Simulate the in situ stress. (**b**) Simulate excavation and tangential stress. 1, stress loader; 2, vertical fixed end; 3, movable door plate; 4, horizontal fixed end; 5, loading platen; 6, specimen


1-Stress loader

2-Vertical fixed end

3-Movable door plate

4- Horizontal fixed end

5- Loading platen

6- Specimen

(a)

(b)
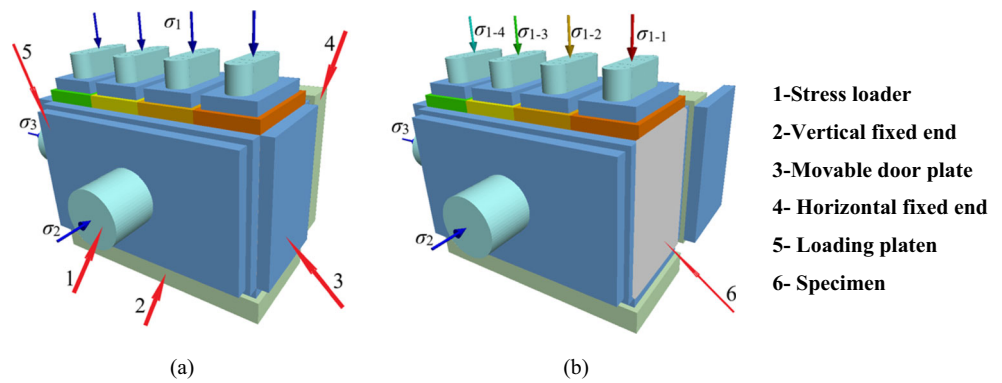
tangential stress gradient, the ejection distance of rockburst debris increased, which indicates that the dynamic failure phenomenon of the specimen rockburst process became increasingly significant, and the rockburst intensity was more remarkable. Moreover, compared with the specimens' lateral crack development after rockburst, the growth lines of lateral cracks in the specimens also showed different variations under different tangential stress gradients. If the tangential stress gradient coefficient was small ($m=0$, $m=2$), cracks propagated parallel to the unloading surface (tensile failure), as shown in

Fig. 13a and b; if $m=4$, cracks were presented as stair-step shape (tensile and shear failure), as shown in Fig. 13c, while $m=6$, cracks were presented as arc shape (shear failure), as shown in Fig. 13d. Therefore, it suggests that the tangential stress gradient affects the crack propagation and failure mechanism of specimen.

From the perspective of energy, at the beginning of the tangential gradient stress loading process, the specimen deformed. The main characteristic of this process was the accumulation of elastic strain energy in the specimen. As the

Fig. 6 Time-history curve of tangential gradient stress loading path: (**a**) $m=0$, (**b**) $m=2$, (**c**) $m=4$, and (**d**) $m=6$


(a)

(b)

(c)

(d)
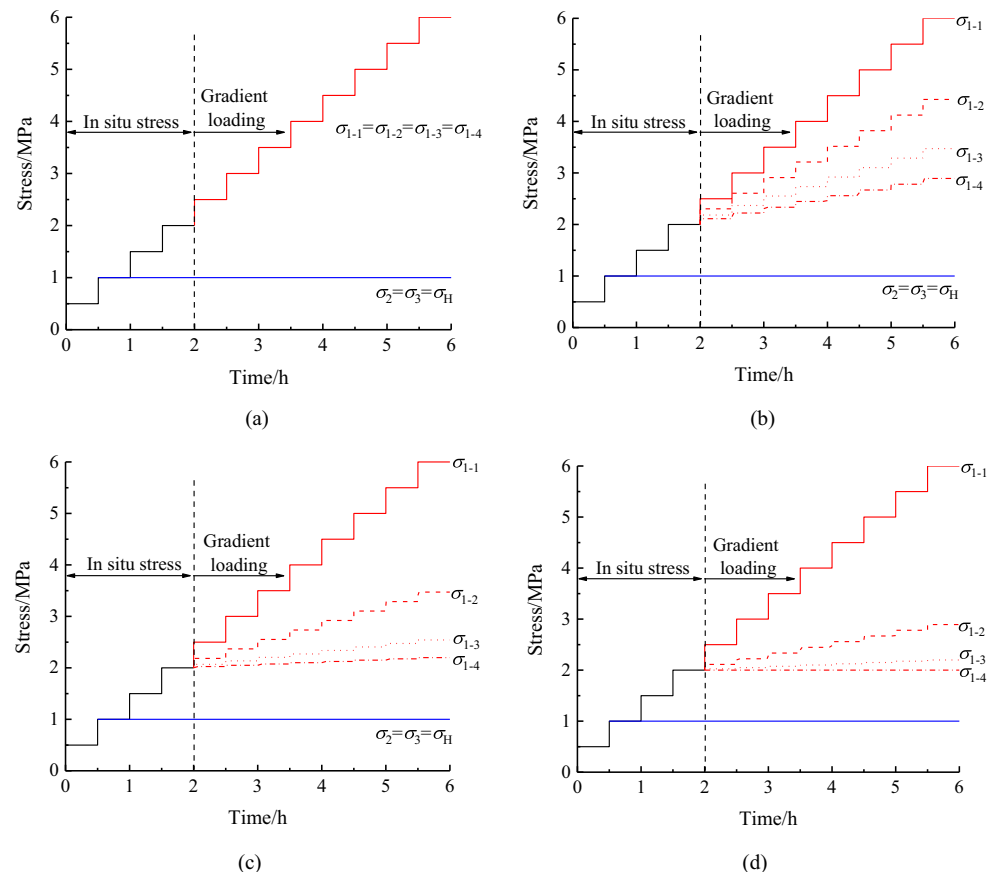
Fig. 7 The measured stress
curves of the specimen with the
loading process: (**a**) $m=0$, (**b**)
$m=2$, (**c**) $m=4$, and (**d**) $m=6$

(a)

(b)

(c)

(d)
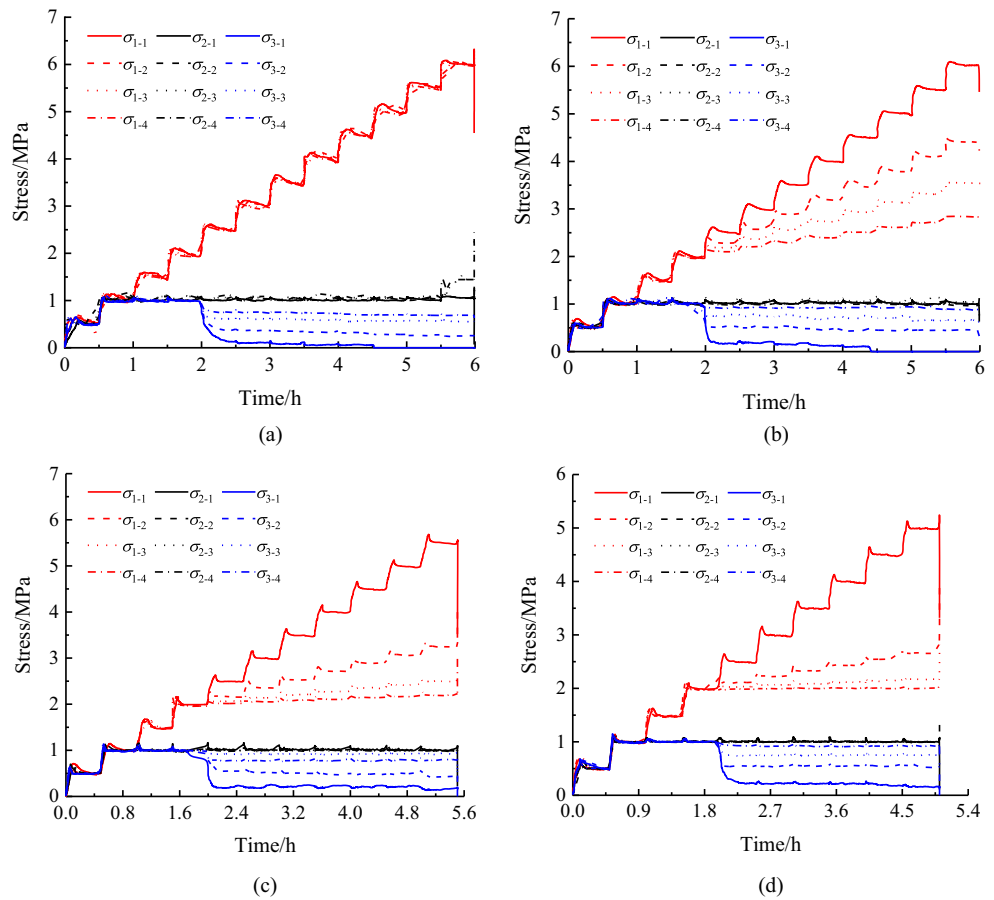
loading process continued, the crispy sound of crepitation occurred inside the specimen, indicating that microcracks were generated and expanded inside the specimen. In this process, in addition to the continuously increased elastic strain energy, part of the work done by external forces was converted into dissipated energy in the specimen, and the dissipation of elastic strain energy accompanied the damage of the specimen. As the loading continues, the elastic strain energy of the specimen was stored to a certain extent, trying to follow a direction (σ_3 direction) that was easy to release. When the

energy released in this direction reached the energy required for the rupture of rock units, the specimen broke down along the σ_3 direction, forming a rockburst. The main characteristic of this process was the release of elastic strain energy. Therefore, in terms of energy, the inoculation and evolution process of strain rockburst could be summarized as a process of elastic strain energy accumulation (specimen elastic deformation)-energy accumulation and dissipation (microcrack expansion, specimen damage)-energy release (macroscopic crack penetration, specimen rockburst failure).

(a)

(b)

(c)

(d)
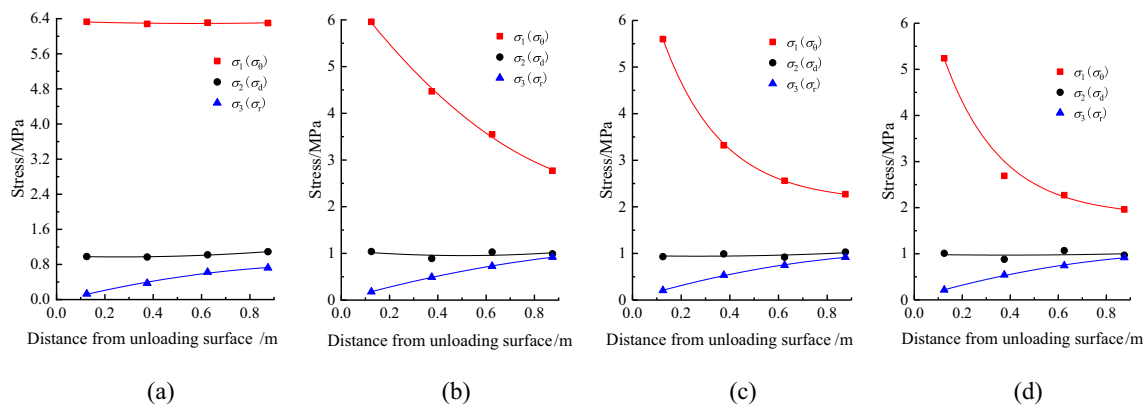
Fig. 8 The measured stress in the specimen with the distance of unloading surface during specimen failure: (**a**) $m=0$, (**b**) $m=2$, (**c**) $m=4$, and (**d**) $m=6$

(a) (b) (c)

Fig. 9 Failure phenomena of specimens at different loading moments (*m*=0): (**a**) 9360s, (**b**) 14040s, and (**c**) 19817s
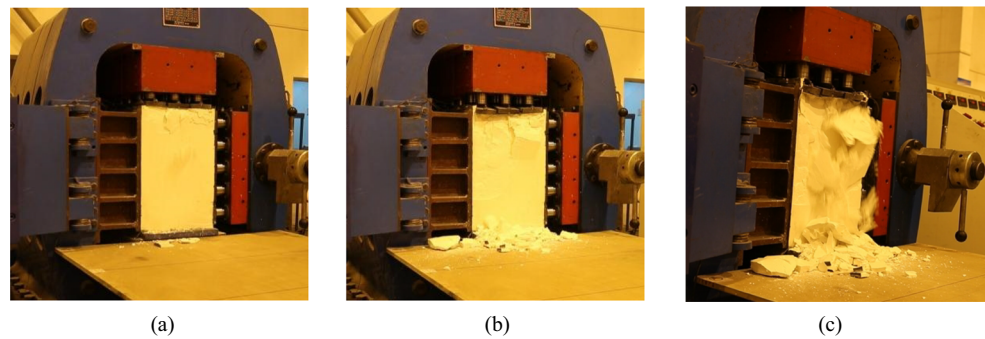
Energy evolution characteristics of specimen rockburst

Energy evolution process based on the strength eigenvalue of specimen rockburst

Liu et al. (2019) analyzed the dissipation and release process of rockburst energy by the AE energy of the rockburst test under different tangential stress gradient loading. Still, AE energy is not the energy in a physical sense. From the microscopic point of view, AE signals are the elastic wave released by internal crack generation, propagation, and fracture of the rock under loading, which can well reflect the rock failure evolution (Cai et al. 2007; Li and Nordlund 1993). AE counts can reflect the degree of microcrack propagation in the specimen. According to the evolution of crack propagation during the specimen failure, it is possible to determine several essential strength eigenvalues of the rockburst process, that is, the crack closure strength (σ_{cc}), the crack initiation strength (σ_{ci}), and the crack damage strength (σ_{cd}). The crack initiation strength (σ_{ci}) refers to the initiation of cracks in the rock, and the crack damage strength (σ_{cd}) represents the beginning of dilation when cracks gradually expand and connect (Brace et al. 1966). This section will analyze the influence of tangential stress gradient on the energy accumulation, dissipation, and release of strainburst in surrounding rock from the perspective of the difference of specimen strength eigenvalue under different tangential gradient stress loading.

Figure 14 is the strength eigenvalue obtained by drawing the AE counts of 4 different tangential gradient stress loading processes in the model test (Liu et al. 2018a).

It can be seen from Fig. 14 that the AE counts have major phase characteristics. At each phase of the curve, the inflection point corresponds to the stress strength eigenvalue of the specimen during rockburst failure, that is, the crack closure strength (σ_{cc}), the crack initiation strength (σ_{ci}), and the crack damage strength (σ_{cd}). At the initial phase ($\sigma_{1\text{-}1} \leq \sigma_{cc}$), the loading conditions of each specimen are the same, the specimen is in the compaction phase, the AE counts show a small section of growth, and its end is corresponding to the closure strength σ_{cc}. σ_{cc} of each specimen is about 1 MPa; and then, the AE counts experience the linear growth phase ($\sigma_{cc} < \sigma_{1\text{-}1} \leq \sigma_{ci}$). The AE counts have a noticeable "low emission period," which lasts a long time, and the specimen is mainly in the elastic strain energy accumulation phase. As the loading continues, when the crack initiation strength σ_{ci} transits to the crack damage strength σ_{cd}, since the internal damage of the specimen begins to form, the AE counts experience an apparent "fluctuation period." In this phase, while the specimen is accumulating energy, the internal micro-fracture initiation leads to energy dissipation, which corresponds to the phase of energy dissipation in the inoculation process of rockburst. When the damage accumulates to a certain extent, the AE counts drop rapidly and go through a short "quiet period." Afterwards, the corresponding AE counts suddenly rise immediately, corresponding to the rapid penetration and generation of cracks, and the specimen internal cracks appear unstable propagation.

Fig. 10 Failure phenomena of specimens at different loading moments (*m*=2): (**a**) 15480s, (**b**) 19074s, and (**c**) 19075s

(a) (b) (c)
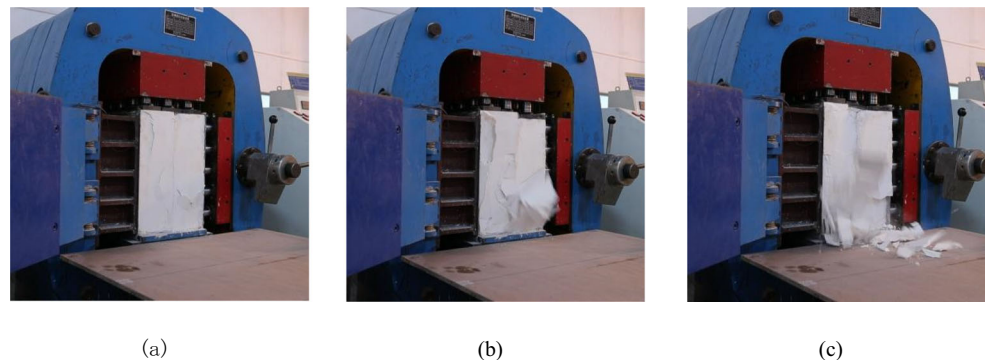
Fig. 11 Failure phenomena of specimens at different loading moments (*m*=4): (**a**) 18766s, (**b**) 18767s, and (**c**) 18768s
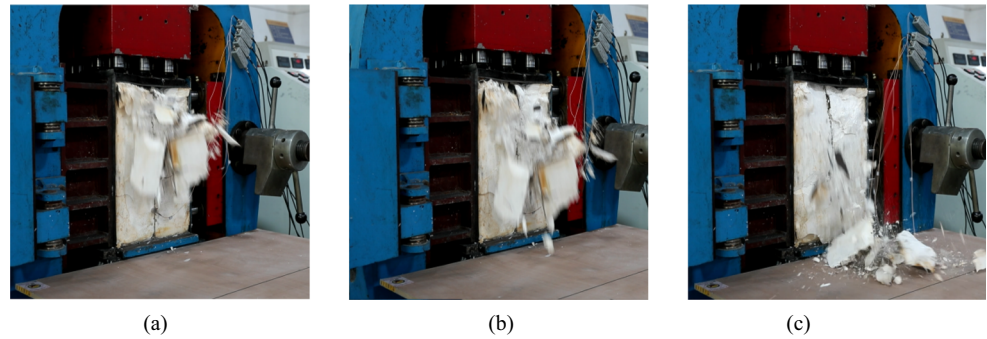
At this point, rockburst enters the phase of energy release; the main fracture in the specimen is broken through, and the fractured rock mass falls and ejects, resulting in full rockburst damage.

To compare and analyze the energy characteristics of each phase of specimen failure under different tangential gradient stress, the ratios (σ_{ci}/σ_f, σ_{cd}/σ_f and σ_{cd}/σ_f -σ_{ci}/σ_f) of the strength eigenvalue to the failure stress σ_f (the maximum value of the tangential gradient stress during rockburst, namely, $\sigma_{1\text{-}1}$ stress) in relation to the tangential stress gradient coefficient *m* are shown in Fig. 15.

As can be seen from Fig. 15, σ_{ci}/σ_f increases gradually with the increase of the tangential stress gradient. The loading phase prior to σ_{ci} corresponds to the accumulation phase of the elastic strain energy of the specimen, which indicates that with the increase of the tangential stress gradient, the energy accumulation phase is relatively longer. Also, σ_{cd}/σ_f -σ_{ci}/σ_f becomes smaller as the tangential stress gradient increases and the ratio corresponds to the energy dissipation phase, meaning that with the increase of the tangential stress gradient, the energy dissipation phase before the rockburst is relatively short. Besides, σ_{cd}/σ_f increases with the increase of the tangential stress gradient. The posterior part of σ_{cd} corresponds to the energy release phase, which shows that the crack instability stage shortens and the energy release rate increases.

The above results indicate that with the increase of the tangential stress gradient, the energy accumulation period in the loading process of the specimen is longer, while the dissipation period is shorter, and the energy release rate becomes larger. The difference in energy accumulation, dissipation,

and release in each phase is the dominant mechanism for the rockburst intensity increasing.

Energy evolution characteristics based on AE *b*-value

To further study the energy characteristics of the specimen rockburst from the perspective of rupture, this section analyzes the characteristics of the AE *b*-value in the specimen's loading process. The AE *b*-value is often used in the field of seismic research, which reflects the evolution process of microcracks and propagation inside the rock (Kim et al. 2015). The AE *b*-value tends to be stable in a specific range, indicating that the state of microcrack failure in the material is relatively constant. In contrast, if the AE *b*-value suddenly jumps over a wide range, it represents the intense change of the microcrack state, suggesting a burst instability expansion. The increases (decreases) of the AE *b*-value indicate that the material's internal micro-fracture is dominated by small-scale (large-scale) failure. There are numerous AE signal activities similar to seismic activities in the rockburst process (Liu et al. 2018b). Therefore, analyzing the AE *b*-value in the rockburst process can study the specimen failure and energy evolution law in the rockburst process.

In this section, the AE amplitude (dB) monitored during the test is divided by 20 to replace the earthquake magnitude (Gutenberg and Richter 1944), that is:

$$M_L = m_s/20 \tag{2}$$

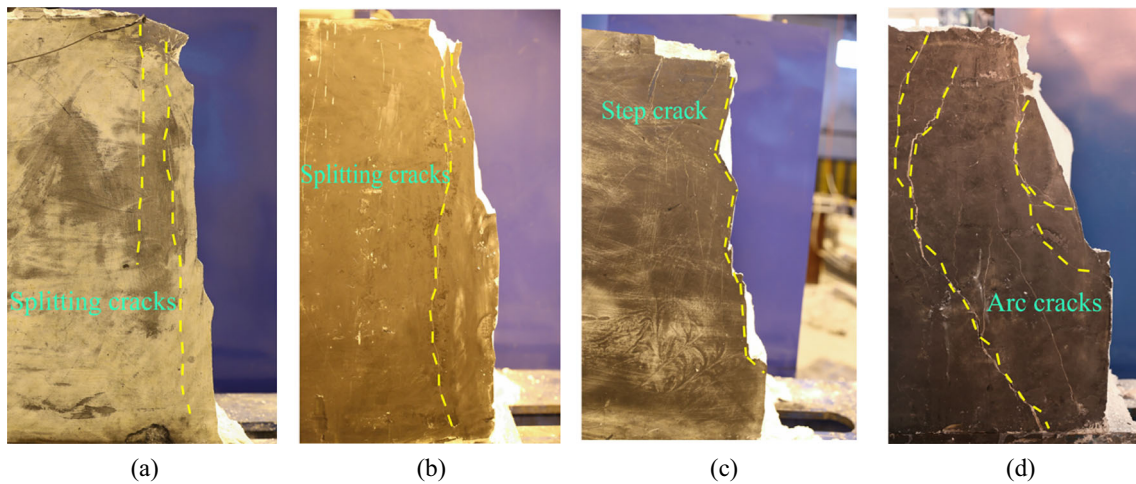**Fig. 12** Failure phenomena of specimens at different loading moments (*m*=6): (**a**) 18492s, (**b**) 18493s, and (**c**) 18494s
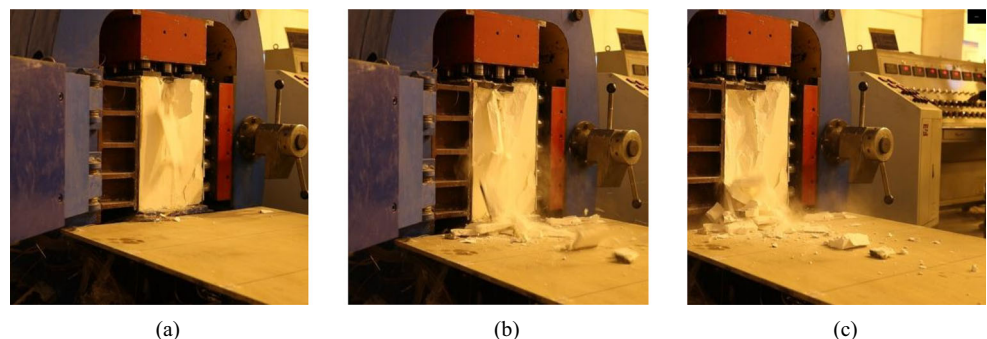
Fig. 13 Lateral crack propagation patterns of specimens at the end of loading: (**a**) *m*=0, (**b**) *m*=2, (**c**) *m*=4, and (**d**) *m*=6

where M_L is equal to the "earthquake magnitude" in the test process and m_S is the AE amplitude (dB) obtained during the test.

Therefore, the relation between earthquake magnitude and frequency, namely, the famous *G-R* relation, can be expressed as (Gutenberg and Richter 1944):

$$lgN = a - bM_L \quad (3)$$

where N is the number of cumulative AE events whose peak amplitude of AE signal is greater than M_L and a and b are constants.

In this section, linear least square method is adopted to calculate AE *b*-value, and the statistical formula for AE *b*-value is (Gutenberg and Richter 1944):

$$b \frac{\sum M_i \sum lgN_i - \Delta m \sum M_i \sum lgN_i}{\Delta m \sum M_1^2 - (\sum M_i)^2} \quad (4)$$

Fig. 14 AE counts and strength eigenvalue under different tangential gradient stress: (**a**) *m*=0, (**b**) *m*=2, (**c**) *m*=4, and (**d**) *m*=6
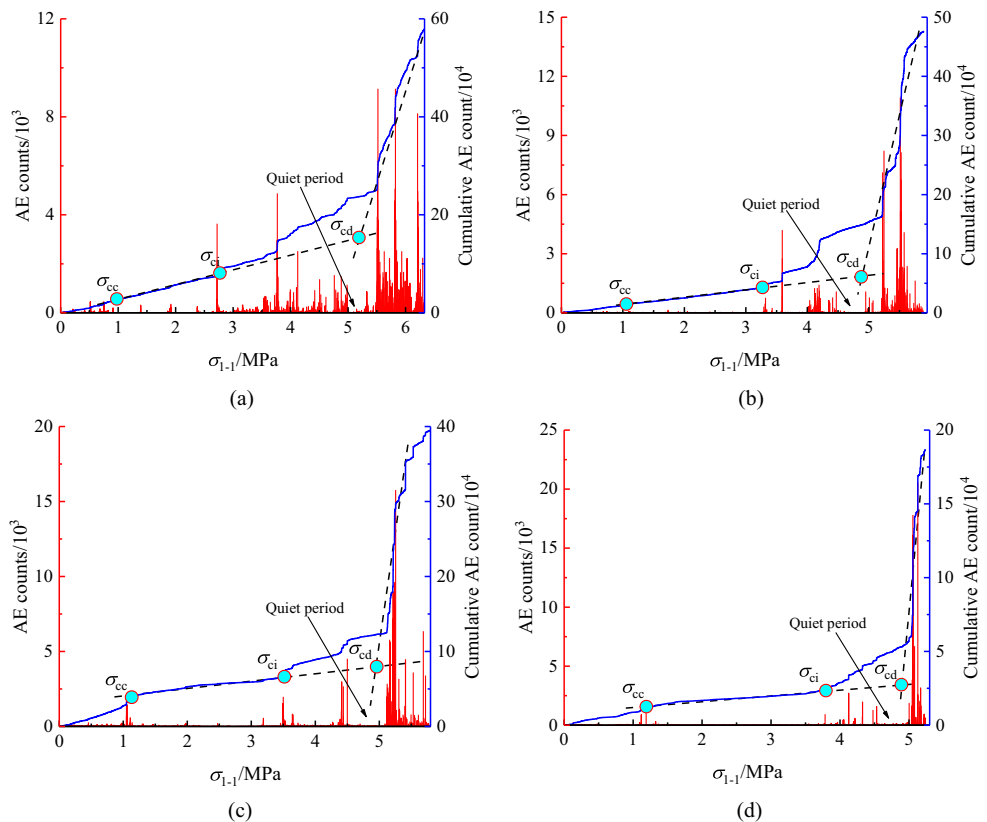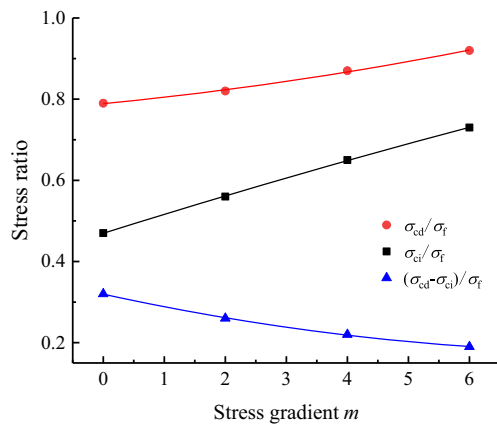
Fig. 15 Variation curve of the ratio of strength eigenvalue to failure stress with tangential stress gradient coefficient

where Δm is the phase classification for AE events, take $\Delta m = 0.5$dB, M_i is the median number of AE events in phase i, and i is the classification number of AE data.

To avoid the decrease of the credibility of the estimate attributable to the small calculation range, every 300 AE events are set as a calculation phase. Then the AE event frequency N during this time and the average energy value representing the magnitude is calculated. Equation (4) is used to get the AE b-value. Ultimately, the AE b-value-the AE amplitude-time curve is obtained, as shown in Fig. 16.

As can be seen from Fig. 16, the overall level of AE b-value is related to the tangential stress gradient. Before the rockburst, when the tangential stress gradient coefficient $m=0$ and $m=2$, the average AE b-value is 0.82 and 0.96, respectively. At this time, the proportion of large-scale microcracks increases, and the proportion of energy dissipation is large. Moreover, the AE b-values show a small continuous fluctuation, reflecting that the microcracking state is slowly changing, consistent with the experimental phenomenon, representing a gradual steady propagation process, and also indicating continuous energy dissipation inside the specimen before rockburst. As the tangential stress gradient coefficient $m=4$ and $m=6$, the average AE b-value is 1.08 and 1.25, respectively, indicating that before rockburst failure, the specimen's internal crack scale is relatively small, and the energy consumption is less. Furthermore, the AE b-values suddenly transit in a wide range, indicating the discontinuous generation of rupture instability.

The results of Lei et al. (2000) show that the physical mechanism of the decrease of AE b-value before rock failure and instability is that the micro-break is changed from tensile failure to shear failure, and the crack interaction is obviously enhanced. The combination of these two factors makes the large event increase obviously and the AE b-value decrease. It can be seen from Fig. 16 that when rockburst failure, with small tangential stress gradient loading ($m=0$, $m=2$), the AE b-value decreases slightly, indicating that the specimen failure is

dominated by tensile failure (consistent with the experimental phenomenon). Tensile failure is a low-stress brittle failure, and only the fracture surface releases energy. Part of the fracture surface's energy is consumed during the fracture development process, and part of it is transferred to the nearby specimen body. Therefore, the overall energy release rate is low, and the rockburst intensity is small. With the increase of the tangential stress gradient ($m=4$, $m=6$), the AE b-value shows a relatively rapid decline, indicating that the internal cracks of the specimen present a state of unstable expansion, the micro-fracture changes from tensile fracture to shear fracture (consistent with the experimental phenomenon), and the energy release rate increases. Shear failure is a violent failure under the condition of high stress. Not only is the energy release amount of shear failure higher than that of tensile failure, but some specimen bodies outside the failure zone also experience stress drop, so the energy release rate is higher and the rockburst intensity is larger.

Probability density distribution of AE Energy

To further study the energy characteristics of the specimen rockburst under tangential gradient stress, the probability density of AE energy is used to reveal the energy magnitude and distribution range of AE events in the process of specimen rockburst (Xie et al. 2017). The energy of an AE event can be defined as the integral of the voltage U squared of the acquisition signal within the duration of the signal, which can be expressed as follows:

$$E = \frac{1}{R} \int_{t_i}^{t_j} U^2(t) dt \qquad (5)$$

where t_i and t_j are respectively the beginning and end time of AE signals and R is the AE equipment's internal resistance value.

Based on AE signals of rockburst under different tangential gradient stress loading conditions, the probability density distribution of AE energy in the logarithmic coordinate can be expressed as (Castillo-Villa et al. 2013):

$$P(Ed)dE \approx \frac{E^{-r}}{E_{min}^{1-r}E} dE, E > E_{min} \qquad (6)$$

where E_{min} is a standardized parameter (Bauke 2007) and r is a critical index.

Figure 17 shows the probability density distribution of AE energy in the specimen rockburst under different tangential stress gradients. It can be seen from Fig. 17 that in double logarithmic coordinates, the overall distribution of AE signals under different tangential stress gradients shows a good linear relationship, and the AE energy can better meet Gutenberg-Richter law (Utsu 1999). The slope r of the probability density function refers to the distribution index of AE energy,
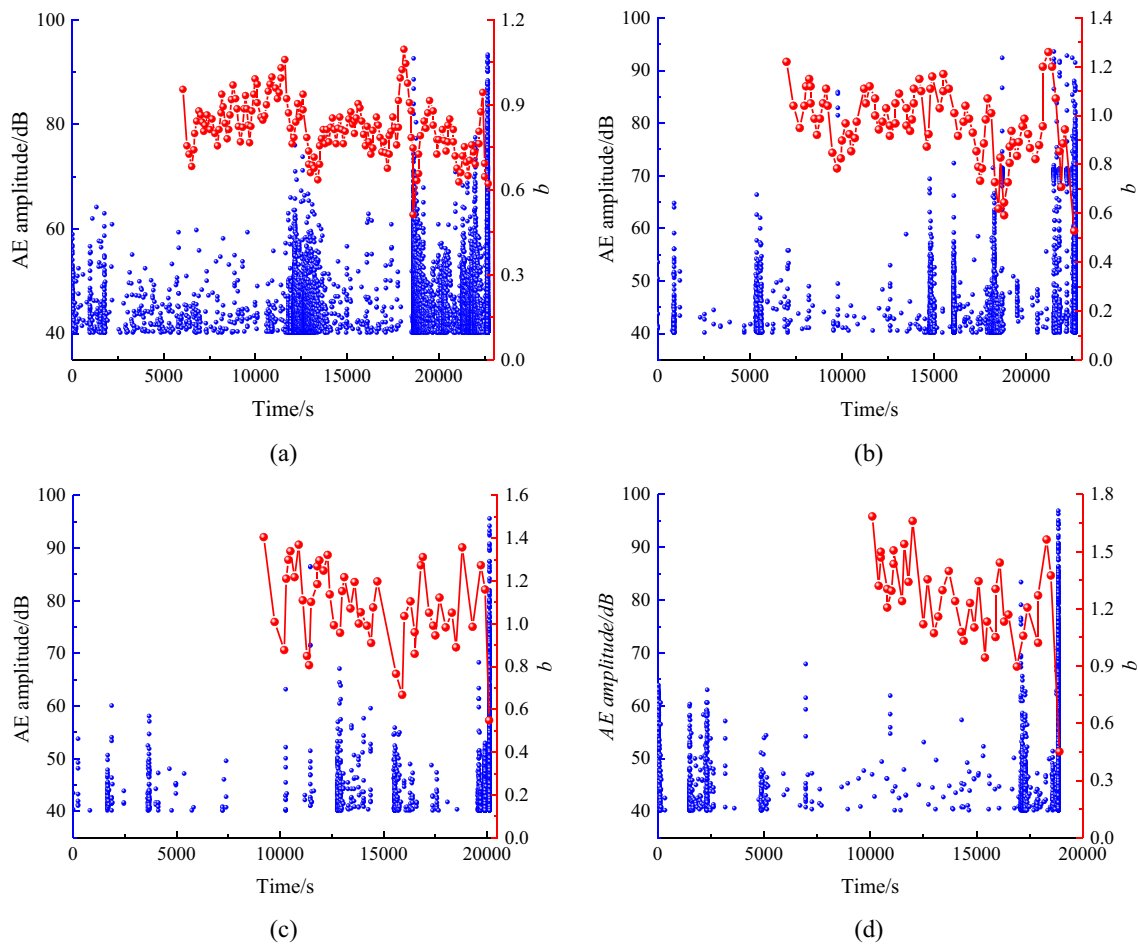
Fig. 16 AE *b*-value and AE amplitude during rockburst failure under different tangential stress gradient: (**a**) *m*=0, (**b**) *m*=2, (**c**) *m*=4, and (**d**) *m*=6

indicating that the data points under different gradient stress loading conditions can better satisfy the power function's attenuation law (also known as the critical index, since it satisfies power-law distribution). AE energy distribution in time
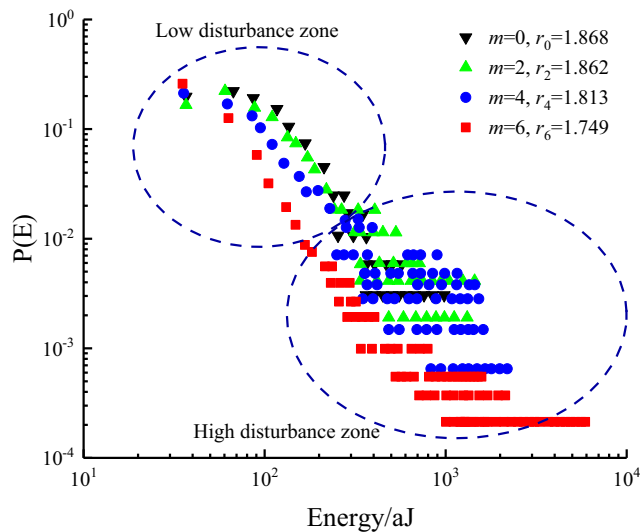
Fig. 17 Distribution of probability density of rockburst energy under different tangential stress gradient loading

is mainly divided into two regions (Travesset et al. 2002): low disturbance zone, at the initial phase of specimen loading, the specimen is less damaged, the AE events are less, and the energy value is small and stable. High disturbance zone: during the loading process, due to fracture expansion and internal structure heterogeneity, a large amount of energy is released into the system, resulting in a sharp increase in AE events. Moreover, the energy value has a large span, and its fluctuation is also large, and the corresponding probability density is small.

Different tangential stress gradient loading which mainly affects the representation scale invariance is the critical index (*r*). Under the conditions of *m*=0 and *m*=2, the critical index of the specimen r_0=1.878 and r_2=1.862, respectively. The probability density of AE energy in the low disturbance zone is more extensive, which indicates that the AE events are more frequently happening and the energy value is small (the energy interval is 10~10^2). The energy dissipation rate before rockburst is higher, but the whole is in the lower energy zone. AE energy has a smaller span ($<10^3$) after entering the high disturbance zone. This indicates that the possibility of higher energy AE events in the process of specimen rockburst is

reduced. With the increase of the tangential stress gradient, the value of r decreases gradually. While the tangential stress gradient coefficient reaches m=4 and m=6, the critical index of the specimen is r_4=1.813, r_6=1.749, respectively. The probability density of AE energy in the specimen's low disturbance zone decreases obviously, which indicates that the energy dissipation rate is low and the overall energy intensity is not high in the early phase of specimen loading. AE energy has a larger span (10^3~10^4) after entering the high disturbance zone. It shows that the probability of high energy AE events in specimen failure is relatively large under a large tangential stress gradient, and the AE energy span is large after entering the high disturbance zone, which indicates that the specimen crack propagation is unstable. The number of AE events increases sharply with the increase of the tangential stress gradient.

Conclusions

In this paper, the effects of tangential stress gradient on specimen rockburst failure and energy evolution were studied by model test with 4 different tangential gradient stress loading. Significant findings are as follows:

(1) The hydraulic-pneumatic composite and tangential gradient stress loading rockburst test can, to a certain extent, represent the change process of tangential and radial tangential stress gradient of deep surrounding rock under excavation disturbance. The phenomenon and stress of the specimen rockburst test are similar to those of actual surrounding rock when rockburst occurs. It shows that the rockburst model test in this paper can reflect the characteristics of rockburst on site.

(2) Specimen rockburst is a process of stress adjustment, deformation by stress (cumulative elastic strain energy)-crack initiation and propagation (energy dissipation)-crack penetration and debris ejection (energy release). With the increase of tangential stress gradient, the energy accumulation period of specimen rockburst becomes longer, and the dissipation period and the energy release period become shorter, which is the main reason for the increase of energy release rate and the enhancement of the rockburst dynamic phenomenon.

(3) The larger the loading tangential stress gradient, the higher the overall level of the AE b-value before rockburst failure, but the worse the continuity, which indicates that the specimen's failure scale is smaller and discontinuous, and the energy dissipation is lower. Also, the larger the loading tangential stress gradient, the larger the AE b-value decreases and the faster the rate decreases, indicating that the specimen is turned from main tensile failure to shear failure and the energy release rate increases when the specimen rockburst.

(4) The AE energy data points of the specimen under different tangential stress gradient can well fill the decay law of power function. The effect of the tangential stress gradient mainly affects the critical index r, which represents the scale invariance. With the increase of the tangential stress gradient of the specimen, the critical index r tends to decrease, and the probability density of AE energy of the corresponding specimen in the low disturbance zone becomes smaller, while the energy span and energy level of the high disturbance zone become larger. Therefore, the periodic variation characteristics of probability density distribution of AE energy under different tangential stress gradient reflect rockburst's energy evolution process.

The article is original, has not been published previously, and has been written by the stated authors who are all aware of its content and approve its submission. It is not under consideration for publication elsewhere, no conflict of interest exists, and if accepted, the article will not be published elsewhere in the same form, in any language, without the written consent of the publisher.

Declarations

Conflict of interest The authors declare no competing interests.

References

Bauke H (2007) Parameter estimation for power-law distributions by maxi-mum likelihood methods. The European Physical Journal B 58:167–173. https://doi.org/10.1140/epjb/e2007-00219-y

Brace WF, Paulding JBW, Scholz CH (1966) Dilatancy in the fracture of crystalline rocks. J Geophys Res 71(16):3939–3953. https://doi.org/10.1029/jz071i016p03939

Brown ET, Hoek E (1978) Trends in relationships between measured in-situ stresses and depth. Int J Rock Mech Min Sci Geomech Abstr 15(4):211–215. https://doi.org/10.1016/0148-9062(78)91227-5

Cai M, Kaiser PK, Morioka H, Minami M, Maejima T, Tasaka Y, Kurose H (2007) FLAC/PFC coupled numerical simulation of AE in large-scale underground excavations. Int J Rock Mech Min Sci 44(4):550–564. https://doi.org/10.1016/j.ijrmms.2006.09.013

Castillo-Villa PO, Baró J, Planes A, Salje EKH, Sellappan P, Kriven WM, Vives E (2013) Crackling noise during failure of alumina under compression: the effect of porosity. J Phys Condens Matter 25(29):292202. https://doi.org/10.1088/0953-8984/25/29/292202

Chen ZY, Su GS, Ju JW, Jiang JQ (2019) Experimental study on energy dissipation of fragments during rockburst. Bull Eng Geol Environ 78(7):5369–5386. https://doi.org/10.1007/s10064-019-01463-9

Feng XT, Zhang XW, Kong R, Wang G (2016) A novel mogi type true triaxial testing apparatus and its use to obtain complete stress-strain curves of hard rocks. Rock Mech Rock Eng 49(5):1649–1662. https://doi.org/10.1007/s00603-015-0875-y

Feng XT, Pei SF, Jiang Q, Zhou YY, Li SJ, Yao ZB (2017) Deep fracturing of the hard rock surrounding a large underground cavern subjected to high geostress: in situ observation and mechanism analysis. Rock Mech Rock Eng 50(8):2155–2175. https://doi.org/10.1007/s00603-017-1220-4

Gutenberg B, Richter CF (1944) Frequency of earthquakes in California. Bull Seismol Soc Am 34(4):185–188. https://doi.org/10.1038/156371a0

He MC, Jia XN, Coli M (2012) Experimental study of rockbursts in underground quarrying of carrara marble. Int J Rock Mech Min Sci 52(6):1–8. https://doi.org/10.1016/j.ijrmms.2012.02.006

He MC, Zhao F, Cai M (2015a) A novel experimental technique to simulate pillar burst in laboratory. Rock Mech Rock Eng 48(5):1833–1848. https://doi.org/10.1007/s00603-014-0687-5

He MC, LR ES, Miranda T, Zhu GL (2015b) Rockburst laboratory tests database-application of data mining techniques. Eng Geol 185:116–130. https://doi.org/10.1016/j.enggeo.2014.12.008

Hou GY, Li XR, Liang HY, Liang JP, Zhou MH, Cui YK (2018) Research on the proportion of high-strength gypsum material and its application in excavation unloading test of surrounding rock specimen (thick wall cylinder). Rock Soil Mech 39(S1):159–166. https://doi.org/10.16285/j.rsm.2017.2059

Huo MZ, Xia YY, Liu XQ, Lin MQ, Wang ZD, Zhu WH (2020) Evolution characteristics of temperature fields of rockburst samples under different stress gradients. Infrared Phys Technol 109:103425. https://doi.org/10.1016/j.infrared.2020.103425

Kaiser PK, Yazici S, Maloney S (2001) Mining-induced stress change and consequences of stress path on excavation stability-a case study. Int J Rock Mech Min Sci 38(2):167–180. https://doi.org/10.1016/S1365-1609(00)00038-1

Kim JS, Lee KS, Cho WJ, Choi HJ, Cho GC (2015) A comparative evaluation of stress-strain and acoustic emission methods for quantitative damage assessments of brittle rock. Rock Mech Rock Eng 48(2):495–508. https://doi.org/10.1007/s00603-014-0590-0

Lei XL, Kusunose K, Rao MVMS, Nishizawa O, Satoh T (2000) Quasi-static fault growth and cracking in homogeneous brittle rock under triaxial compression using acoustic emission monitoring. J Geophys Res 105(B3):6127–6139. https://doi.org/10.1029/1999JB900385

Li C, Nordlund E (1993) Experimental verification of the Kaiser effect in rocks. Rock Mech Rock Eng 26(4):333–351. https://doi.org/10.1007/BF01027116

Li C, Mikula P, Simser B, Hebblewhite B, Joughin W, Feng XW, Xu NW (2019) Discussions on rockburst and dynamic ground support in deep mines. J Rock Mech Geotech Eng 11(5):1110–1118. https://doi.org/10.1016/j.jrmge.2019.06.001

Liu P, Ju Y, G. Ranjith P, Zheng ZM, Chen JL (2016) Experimental investigation of the effects of heterogeneity and geostress difference on the 3D growth and distribution of hydrofracturing cracks in unconventional reservoir rocks. Journal of Natural Gas Science and Engineering 35:541-554. https://doi.org/10.1016/j.jngse.2016.08.071

Liu QS, Wei L, Lei GF, Liu Q, Liu H (2018a) Experimental study on crack initiation damage strength and brittle parameter evolution of sandstone. Chinese Journal of Geotechnical Engineering 40(10):1782–1789. https://doi.org/10.11779/CJGE201810004

Liu XX, Liang ZZ, Zhang YB, Liang P, Tian BZ (2018b) Experimental study on the monitoring of rockburst in tunnels under dry and saturated conditions using AE and infrared monitoring. Tunn Undergr Space Technol 82:517–528. https://doi.org/10.1016/j.tust.2018.08.011

Liu XQ, Xia YY, Lin MQ, Benzerzour M (2019) Experimental study of rockburst under true-triaxial gradient loading conditions. Geomechanics and Engineering 18:28–40. https://doi.org/10.12989/gae.2019.18.5.481

Mansurov VA (2001) Prediction of rockbursts by analysis of induced seismicity data. Int J Rock Mech Min Sci 38(6):893–901. https://doi.org/10.1016/S1365-1609(01)00055-7

Peng RD, Ju Y, Gao F, Xie HP, Wang P (2014) Energy analysis on damage of coal under cyclical triaxial loading and unloading conditions. J China Coal Soc 39(02):245–252. https://doi.org/10.13225/j.cnki.jccs.2013.2010

Qian QH (2014) Definition, mechanism, classification and quantitative prediction model of rock burst and rockburst. Rock Soil Mech 35(1):1–6. https://doi.org/10.16285/j.rsm.2014.01.028

Si XF, Gong FQ (2020) Strength-weakening effect and shear-tension failure mode transformation mechanism of rockburst for fine-grained granite under triaxial unloading compression. Int J Rock Mech Min Sci:131. https://doi.org/10.1016/j.ijrmms.2020.104347

Simser BP (2019) Rockburst management in Canadian hard rock mines. J Rock Mech Geotech Eng 11(5):1036–1043. https://doi.org/10.1016/j.jrmge.2019.07.005

Singh AK, Singh R, Maiti J, Kumar R, Mandal PK (2011) Assessment of mining induced stress development over coal pillars during depillaring. Int J Rock Mech Min Sci 48(5):805–818. https://doi.org/10.1016/j.ijrmms.2011.04.004

Su GS, Chen ZY, Ju JW, Jiang JQ (2017a) Influence of temperature on the strain burst characteristics of granite under true triaxial loading conditions. Eng Geol 222:38–52. https://doi.org/10.1016/j.enggeo.2017.03.021

Su GS, Feng XT, Wang JH, Jiang JQ, Hu LH (2017b) Experimental study of remotely triggered rockburst induced by a tunnel axial dynamic disturbance under true-triaxial conditions. Rock Mech Rock Eng 50(8):2207–2226. https://doi.org/10.1007/s00603-017-1218-y

Travesset A, White RA, Dahmen KA (2002) Crackling noise, power spec-tra, and disorder-induced critical scaling. Phys Rev B 66:1–11. https://doi.org/10.1103/PhysRevB.66.024430

Utsu T (1999) Representation and analysis of the earthquake size distribution: a historical review and some new approaches. Pure Appl Geophys 155(2-4):509–535. https://doi.org/10.1007/s000240050276

Wang CL, Wu AX, Lu H, Bao TC, Liu XH (2015) Predicting rockburst tendency based on fuzzy matter-element model. Int J Rock Mech Min Sci 75:224–232. https://doi.org/10.1016/j.ijrmms.2015.02.004

Xie KN, Jiang DY, Jiang X, Chen J, Wang JY, Yuan X, Zhou JP (2017) Energy distribution and criticality characteristics analysis of shale Brazilian splitting test. J China Coal Soc 42(03):613–620. https://doi.org/10.13225/j.cnki.jccs.2016.0561

Zhai SB, Su GS, Yin SD, Yan SZ, Wang ZF, Yan LB (2020) Fracture evolution during rockburst under true-triaxial loading using acoustic emission monitoring. Bull Eng Geol Environ 79:1–18. https://doi.org/10.1007/s10064-020-01858-z

Zhang P, Yang CH, Wang H, Guo YT, Xu F, Hou ZK (2018) Stress-strain characteristics and anisotropy energy of shale under uniaxial

compression. Rock Soil Mech 39(6):2106–2114. https://doi.org/10.16285/j.rsm.2016.1824

Zhang W, Feng XT, Xiao YX, Feng GL, Yao ZB, Hu L, Niu WJ (2020) A rockburst intensity criterion based on the Geological Strength Index, experiences learned from a deep tunnel. Bull Eng Geol Environ 79:1–19. https://doi.org/10.1007/s10064-020-01774-2

Zhou H, Xu RC, Lu JJ, Zhang CQ, Meng FZ, Shen Z (2015) Study on mechanisms and physical simulation experiment of slab buckling rockburst in deep tunnel. Chin J Rock Mech Eng 34(S2):3658–3666. https://doi.org/10.13722/j.cnki.jrme.2014.0874

Zhou J, Koopialipoor M, Li EM, Armaghani DJ (2020) Prediction of rockburst risk in underground projects developing a neuro-bee intelligent system. Bull Eng Geol Environ 79(8):1–15. https://doi.org/10.1007/s10064-020-01788-w